processes

MDPI

Article

In Situ Stress Control on Coal Reservoir Permeability and Hydraulic Fracturing Fracture Propagation: A Case Study in Yangquan Mining Area, Northeastern Qinshui Basin, China

Ben Ma [1], Xiaoyang Zhang [1,*], Dawei Lv [1], Miao Liu [1], Xunzhong Du [1], Junjian Zhang [1], Han Wang [2] and Dongdong Wang [1]

[1] College of Earth Sciences & Engineering, Shandong University of Science and Technology, Qingdao 266590, China; maopp@sdust.edu.cn (B.M.); lvdawei95@163.com (D.L.); liumiao703@126.com (M.L.); xunzhong0328@163.com (X.D.); junjianzhang@cumt.edu.cn (J.Z.); wdd02_1@163.com (D.W.)
[2] Shandong University of Science and Technology Library, Qingdao 266590, China; whsdust@126.com
* Correspondence: zhanglsyr@cumt.edu.cn

Abstract

Permeability is the key factor controlling coalbed methane (CBM) production, and hydraulic fracturing is an essential technique for permeability enhancement in low-permeability coal reservoirs. In situ stress plays a dominant role in both coal reservoir permeability evolution and hydraulic fracture propagation. By taking the Yangquan Mining Area in the northeastern Qinshui Basin, China, as the study area, this study integrated injection/falloff well testing and microseismic monitoring data to investigate the controlling effect of in situ stress on coal reservoir permeability and hydraulic fracture geometry. The results show that the in situ stress and reservoir pressure generally increase with burial depth. The measured maximum and minimum horizontal principal stresses ranged from 4.04 to 23.41 MPa and 3.72 to 13.24 MPa, with average values of 14.54 MPa and 8.64 MPa, respectively, while the vertical principal stress ranged from 6.50 to 19.87 MPa, averaging 13.31 MPa. The reservoir pressure ranged from 0.55 to 6.09 MPa, with an average value of 2.32 MPa. The lateral stress coefficient (λ) ranged from 0.45 to 1.68 (average of 0.89), exhibiting a pattern of dispersion in shallow strata and convergence in deeper strata. The regional stress regime is dominated by strike-slip faulting, with approximately 60.5% of the deeper measurement points characterized by σ_H > σ_v > σ_h. The coal seam permeability ranged from 0.03 to 15.52 mD, with an average value of 1.62 mD, and decreased exponentially with increasing effective stress. The controlling effect of the coal seam thickness on the permeability exhibited distinct segmented characteristics. The microseismic monitoring results from 23 hydraulic fracturing treatments indicate that approximately 74% of the fractures trended NE5–NE55°, consistent with the regional maximum horizontal principal stress direction. The fracture lengths ranged from 124.9 to 447.7 m, with an average of 344.7 m, while the fracture heights ranged from 12.9 to 79.09 m. All the induced fractures were predominantly vertical. A greater horizontal principal stress difference was associated with a lower permeability and promoted the formation of longer and more planar hydraulic fractures. These results demonstrate that the regional in situ stress field exerts significant control on both the coal reservoir permeability and hydraulic fracture morphology, providing important guidance for stress-based optimization of CBM development and hydraulic fracturing design.

Keywords: in situ stress; permeability; hydraulic fracturing fractures; stress dependence

Check for updates

Academic Editor: Liyun Yang

Received: 10 March 2026
Revised: 20 May 2026
Accepted: 4 June 2026
Published: 9 June 2026

Copyright: © 2026 by the authors. Licensee MDPI, Basel, Switzerland. This article is an open access article distributed under the terms and conditions of the Creative Commons Attribution (CC BY) license.

1. Introduction

Coalbed methane (CBM), as a critical unconventional natural gas resource, not only serves as a vital supplementary energy source to optimize China's energy structure and enhance national energy supply security, but also plays a key role in reducing greenhouse gas emissions and preventing coal mine gas disasters [1]. As the core parameter controlling the entire process of methane desorption, diffusion and seepage in coal reservoirs, permeability directly determines the productivity of CBM wells and the economic efficiency of development projects. For China's CBM resources, a large proportion are hosted in deep formations with high in situ stress conditions: with the continuous expansion of CBM exploration and development towards deeper layers, the in situ stress level increases significantly with burial depth, leading to a general ultra-low permeability characteristic of coal reservoirs. Statistics show that, in typical high-stress CBM basins such as the Qinshui Basin and Ordos Basin, the permeability of coal seams generally ranges from 0.01 to 1.5 mD, far lower than the development threshold of conventional natural gas reservoirs, which has become the core geological bottleneck restricting the efficient exploitation of deep CBM resources in China [2].

Numerous factors have been confirmed to affect the permeability of coal reservoirs, including the coal rank, pore–fracture structure, reservoir pressure, burial depth and tectonic conditions. Among these factors, in situ stress has been gradually recognized as the core controlling factor, as it directly dominates the opening and closure state of the natural fracture network in coal seams, which is the main flow channel for CBM migration [3–5]. Early classic petrophysical research by Tiab and Donaldson [6] systematically elaborated the stress-sensitivity mechanism of permeability in porous media, laying a solid theoretical foundation for understanding the response of coal permeability to stress changes. On this basis, Palmer and Mansoori established a classic stress-dependent permeability model for coal seams [7], which quantitatively characterized the evolution of coal permeability with effective stress and has been widely applied in global CBM development practices. Subsequent studies have further verified this rule: Zoback et al. revealed through global in situ stress measurement data that the horizontal stress difference is the key factor causing permeability anisotropy in coal reservoirs [3]; domestic scholars such as Gao et al. and Meng et al. also confirmed, based on field test data, that the coal reservoir permeability decreases exponentially with an increase in the in situ stress and that the horizontal principal stress difference directly regulates the heterogeneity of permeability [4,5]. These studies all indicate that clarifying the control effect of in situ stress on permeability is the primary premise for favorable reservoir screening and productivity predictions in high-stress CBM development areas.

To break through the development bottleneck of low-permeability coal reservoirs, hydraulic fracturing has become an essential reservoir stimulation technology for CBM development in China. By injecting high-pressure fluid into coal seams, this technology connects natural fracture systems and generates artificial fracture networks with a high conductivity, thereby effectively improving the seepage capacity of coal reservoirs [2]. A large number of engineering practices have shown that the propagation characteristics of hydraulic fractures, including their orientation, extension scale and morphological structure, directly determine the effect of reservoir reconstruction and the final single-well productivity. However, the initiation and propagation of hydraulic fractures are not arbitrary, but are directly controlled by the in situ stress field: experimental and theoretical analyses confirm that hydraulic fractures tend to propagate perpendicular to the minimum horizontal principal stress, and the magnitude of the horizontal principal stress difference determines whether the fractures remain single and planar or branch into complex networks [8–10]. In recent years, scholars have carried out a large number of in-depth studies

on this issue: Ren et al. confirmed through true-triaxial hydraulic fracturing experiments combined with CT imaging that weak planes and in situ stress jointly control the initiation and propagation of fractures [8]; Shi et al. found through physical model experiments that a high horizontal principal stress difference is conducive to the formation of single long straight fractures, while a low stress difference will promote fracture branching and the formation of complex fracture networks [9]; Lakirouhani and Jolfaei further improved the fracture initiation criterion by incorporating fracture mechanics and a coupled criterion with emphasis on the size effect, providing an important supplement for the accurate prediction of the fracture initiation pressure [10].

Although previous studies have extensively discussed the effects of in situ stress on coal permeability and hydraulic fracture propagation, several issues remain unresolved. First, many existing permeability models or fracture-propagation models are based on single-seam reservoirs, and therefore may not fully reflect the behavior of multi-seam coal reservoirs under complex geological conditions. Second, most previous studies have focused either on stress-controlled permeability or on hydraulic fracture propagation separately, whereas integrated analyses combining in situ stress measurements, field permeability data, and microseismic fracture monitoring remain limited. Third, the applicability of stress–permeability relationships and fracture-propagation mechanisms established in basins other than the Yangquan Mining Area in the northeastern Qinshui Basin still requires further verification. The Yangquan Mining Area is characterized by multiple developable coal seams, relatively deep burial, complex structural conditions, and a low reservoir permeability. Therefore, a systematic investigation of the controlling effect of in situ stress on both the permeability and hydraulic fracture propagation is necessary for guiding multi-seam CBM development in this area.

In this study, the Yangquan Mining Area in the northeastern Qinshui Basin was selected as the research target. Based on injection/falloff well test data, coal reservoir permeability data, and microseismic monitoring data from hydraulic fracturing treatments, this study aimed to: (1) characterize the distribution of the in situ stress field and coal reservoir permeability in different coal seams; (2) analyze the controlling effects of the burial depth, coal seam thickness, coal body structure, and especially in situ stress on the coal reservoir permeability; (3) clarify the relationship between the horizontal principal stress difference and hydraulic fracture morphology, including fracture orientation, height, and length; and (4) reveal the dual control of in situ stress on the coal reservoir permeability and hydraulic fracture propagation. The novelty of this study lies in the integrated use of field stress measurements, well-test permeability data, and microseismic fracture-monitoring results to quantitatively evaluate the stress–permeability relationship and the stress-controlled fracture-propagation mechanism in a multi-seam CBM development area. The results are expected to provide theoretical support and practical guidance for favorable zone selection, hydraulic fracturing design, and efficient CBM development in the Yangquan Mining Area.

2. Geologic Setting

The Yangquan mining area, situated in the northeastern Qinshui Basin on the western flank of the central Taihang Uplift (Figure 1), represents China's largest production base of high-quality anthracite [11]. Regionally, the mining area is characterized by an east-rising, west-dipping monocline with gently dipping strata and structurally complex deformation patterns. In the western sector, the dominant structural geometry is a monocline striking approximately E–W and dipping southward. The northeastern portion contains a strongly deformed structural belt that trends predominantly NE. The southern area is likewise dominated by a monocline that strikes NW and dips toward the SW. Secondary deformation is expressed primarily as folding, accompanied by locally developed high-angle faulting [12].

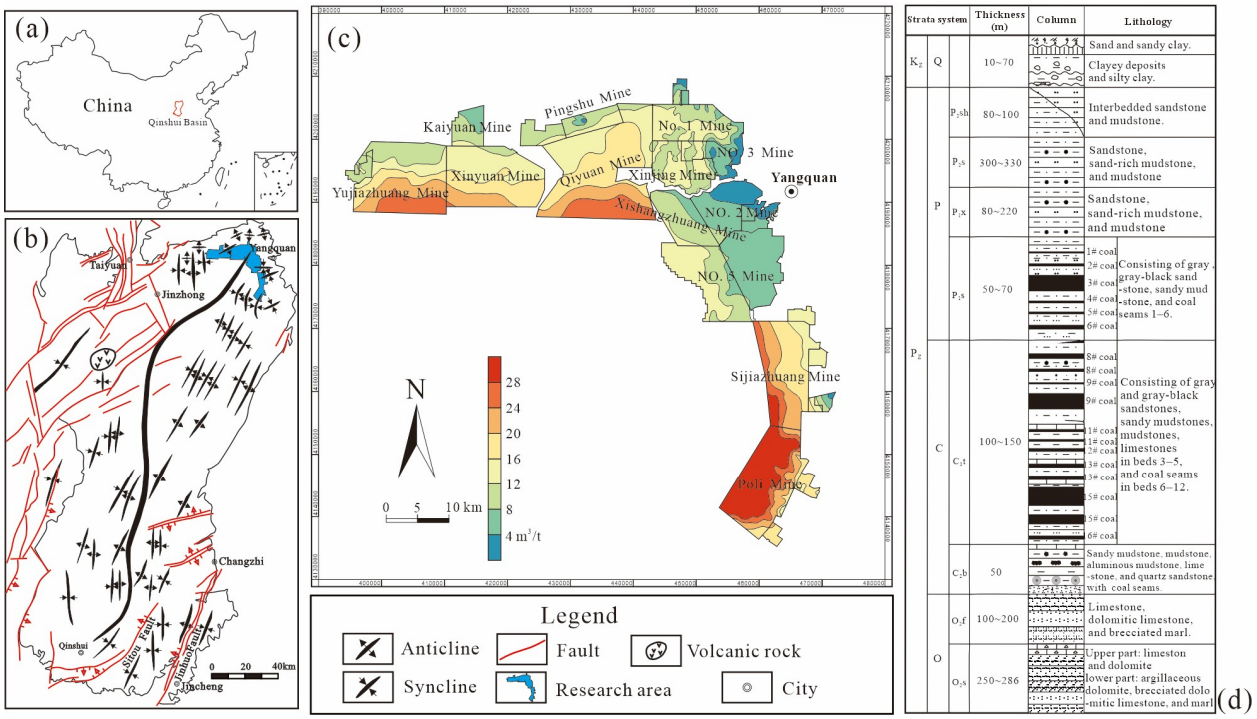

Figure 1. Contour maps showing the gas content in the No. 3 coal seam of the Yangquan area within the Qinshui Basin in North China, along with a sequence columnar diagram of the Ordovician–Quaternary coal-bearing strata. (**a**) Location of the Qinshui Basin within North China. (**b**) Position of Yangquan in the northeastern part of the Qinshui Basin. (**c**) Contour map illustrating the gas content in the Yangquan No. 3 coal seam. (**d**) Stratigraphic columnar diagram of coal-bearing strata. The stratigraphic columnar diagram was compiled based on measured data of test wells and regional stratigraphic data cited from [13].

The principal coal-bearing strata in the study area comprise the Carboniferous–Permian Taiyuan Formation and the Permian Shanxi Formation, with the Shanxi Formation forming the primary productive interval. The Shanxi Formation is lithologically dominated by dark-gray sandy mudstone, mudstone, and grayish-white medium–coarse-grained sandstone. The cumulative coal thickness of the Shanxi Formation averages 3.61 m, with the No. 3 coal seam constituting the principal minable seam. Throughout the mining district, the seam is largely continuous and commercially mineable, serving as the primary CBM-producing interval. The Taiyuan Formation is composed predominantly of gray-white to gray–yellow-green sandy mudstone, medium–coarse-grained sandstone, and limestone interbedded with carbonaceous mudstone. The Taiyuan Formation contains an average cumulative coal thickness of 12.04 m, dominated by the No. 15 coal seam, which averages 6.3 m in thickness and is laterally continuous and mineable across the entire mining district.

The CBM gas content in the Yangquan mining area ranges from 5.76 to 21.66 m^3/t, averaging 10.71 m^3/t. The moisture content varies from 1.23% to 1.43%, with an average value of 1.30%. The ash yield ranges between 14.23% and 23.58%, averaging 20.16%. The volatile matter yield ranges from 10.25% to 12.43%, with an average of 11.74% (Table 1). The maceral assemblages of the coal seams are dominated by vitrinite, which accounts for approximately 66–77% of the total maceral composition, followed by inertinite, whereas liptinite occurs only in trace amounts. The maximum vitrinite reflectance ranges from 2.34% to 2.55%, averaging 2.49%, and the degree of coalification increases systematically with increasing burial depth.

Table 1. Coal seam thickness and coal lithology in study area.

Coal Seam Number	Coal Seam Thickness (m)	Vitrinite Ro (%)	Vitrinite (%)	Inertinite (%)	A_d (%)	V_{daf} (%)	M_{ad} (%)
3#	0.75~4.80 2.26	2.34	66.72	33.28	14.23	10.25	1.23
8#	0.00~3.90 1.65	2.4	75.61	24.39	23.58	12.43	1.24
9#	0.00~4.10 1.90	2.43	65.5	34.5	22.15	12.2	1.25
15#	3.80~9.50 6.30	2.55	77.62	22.38	16.08	10.72	1.43

3. Data and Methods

3.1. Injection/Falloff Well Test and In Situ Stress Measurement

To characterize the coal-reservoir permeability and pressure behavior, and to determine the in situ stress parameters, injection/falloff well testing was employed in this study. Injection/falloff testing is a commonly used single-well pressure-transient method for estimating the in situ permeability, skin factor, and reservoir pressure in coalbed methane reservoirs [14]. During the test, clean water is first injected into the target coal seam at a constant rate below the fracture pressure of the coal seam until the bottom-hole pressure reaches a quasi-steady state. The injection is then terminated abruptly, and the subsequent time-dependent bottom-hole pressure response during shut-in is recorded using a downhole pressure gauge. To reduce the influence of injection-induced stress perturbations on the permeability during the injection/falloff test, the initial injection pressure is generally kept low. After the injection pressure is adjusted, the flow-static injection continues for 12 h, and the well is then shut in for at least 26.5 h, ensuring that the shut-in time is not less than twice the injection time. The initial phase of injection serves to adjust the discharge rate, whereas the middle and later phases correspond to a stabilized injection stage during which the discharge remains essentially constant. During the early part of the shut-in pressure decline, pressure recovery is normal and the curve is smooth; during the later part of the shut-in pressure decline, the pressure is essentially stable (Figure 2). In general, pressure variations during the shut-in stage are smooth and subject to minimal disturbance from changes in the injection discharge, so the pressure-falloff curve is the most representative for interpretation. Accordingly, the pressure data from the shut-in pressure-decline stage were selected for the analysis herein.

The data analysis methods for injection/falloff well testing mainly include straight-line fitting and type-curve analyses. Due to the influence of reservoir characteristics, fluid properties, boundary conditions, and other factors in the study area, some analysis methods and type curves are not applicable. Specifically, classical constant-rate type-curve solutions (such as the Theis solution, the Hantush–Jacob method, and the Neuman method) assume homogeneous, isotropic, single-porosity reservoirs and require a constant injection rate; these assumptions do not hold for injection/fall-off tests in coalbed methane wells. Consequently, all 13 well tests analyzed in this study were interpreted using both semi-log (Horner) plots and log–log diagnostic plots, with pressure-history matching employed to validate the derived parameters. In the semi-log method, the bottom-hole pressure is plotted against the Horner time factor on a semi-logarithmic scale to infer the static reservoir pressure and diagnose the prevailing flow regimes. Using the semi-log fitting method, the initial reservoir pressure can be estimated and used as an initial check for the permeability back-calculation. The log–log fitting method plots pressure versus time during the shut-

in period on a log–log scale and computes the pressure derivative [15]. This approach allows for the clear identification of flow regimes and, through models incorporating wellbore storage and related effects, enables the determination of key formation parameters, including the skin factor, permeability, and reservoir pressure.

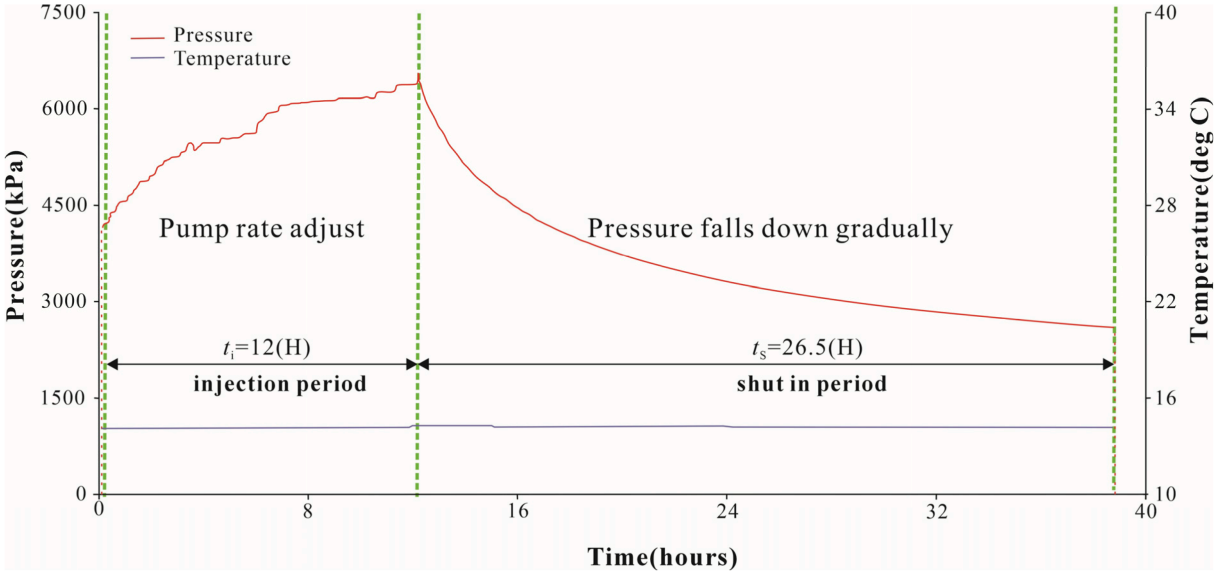

Figure 2. Pressure and time curve of an injection/falloff test well in the study area.

Each in situ stress measurement for the test wells included four cycles, and one or two cycles exhibiting clear fracture initiation and closure behaviors were selected, with the shut-in pressure-drop response analyzed using log–log diagnostic plots or the square-root-of-time method, to obtain reliable estimates of the fracture closure pressure (Figure 3) [16]. In this study, the closure-pressure interpretation for the 13 CBM test wells was uniformly performed using the square-root-of-time approach, in which the bottom-hole pressure or pressure drop is plotted against the square root of the shut-in time to diagnose flow regimes and detect fracture-closure signatures.

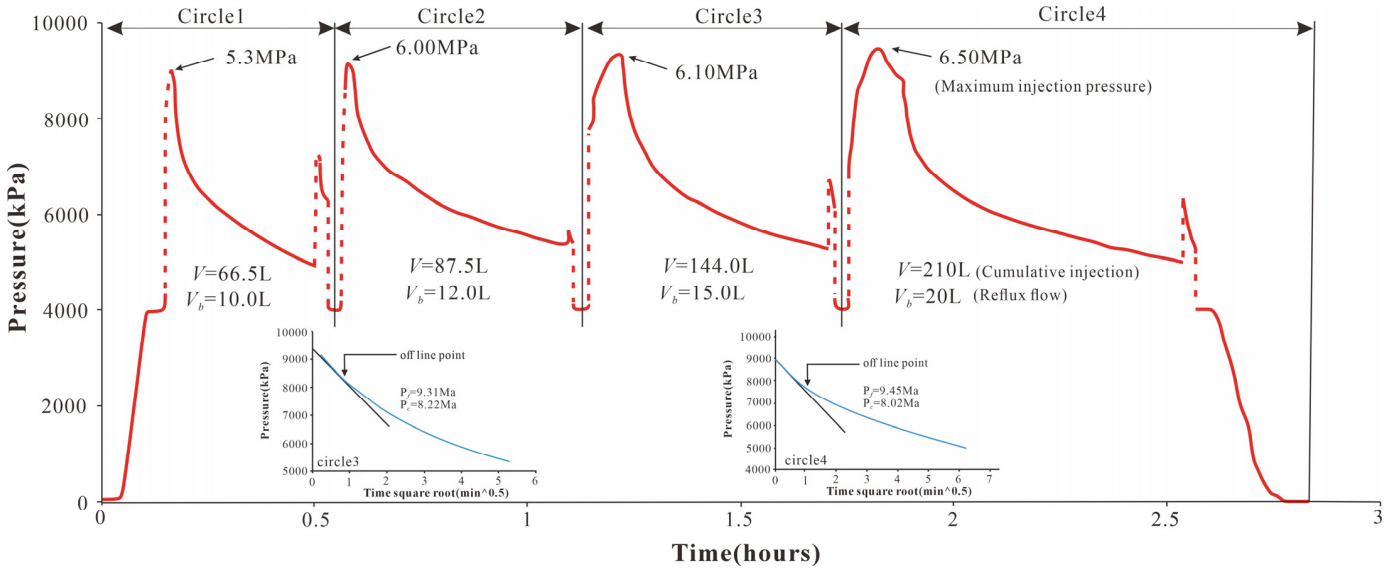

Figure 3. Pressure and time curve of an in situ stress measurement well in the study area.

The breakdown pressure, P_f, refers to the peak bottom-hole pressure required to initiate a new fracture or penetrate pre-existing fractures during continuous injection. It is

affected by multiple factors, including the minimum horizontal stress, pore pressure, tensile strength of the coal/rock, near-wellbore stress concentration, natural fractures, injection rate, and wellbore friction. The fracture pressure is determined from the injection-stage response, whereas the closure pressure is derived from an analysis of the pressure falloff during shut-in. The closure pressure corresponds to the inflection on the pressure-decay curve where the response transitions from linear leak-off behavior to a steeper decline. This point marks the onset of mechanical closure of the fracture faces. The closure pressure is taken to be equal to the minimum horizontal principal stress.

$$\sigma_h = P_c \tag{1}$$

Classical hydraulic fracturing stress measurement theory assumes that the rock is homogeneous, isotropic, and impermeable to fluids, and, based on the Hubbert–Willis formulation together with the fracture pressure analytical method, the maximum horizontal principal stress can be reasonably estimated using the fracture closure pressure, breakdown pressure, reservoir pressure, and tensile strength of the rock [17,18].

$$\sigma_H = 3P_c - P_f - P_0 + T \tag{2}$$

In the equation, σ_H is the maximum horizontal principal stress (MPa); P_c is the closure pressure (MPa); P_f is the breakdown pressure (MPa); P_0 is the reservoir pressure (MPa); and T is the tensile strength (MPa).

The vertical stress σ_v is calculated from the density and thickness of the overburden using the empirical relationship proposed by [19]:

$$\sigma_v = \gamma H \approx 0.027H \tag{3}$$

In the equation, γ is the unit weight of the rock (kN/m^3) and H is the burial depth of the strata (m).

Coal reservoirs are subjected to a three-dimensional stress regime comprising vertical stress and two orthogonal horizontal stresses. The lateral stress coefficient λ is a key parameter describing the relative magnitude of horizontal stress with respect to vertical stress. Its spatial distribution significantly controls coal-reservoir permeability and the propagation behavior of hydraulic fractures.

In the field test, water is injected at a constant rate into the target coal seam through a cased wellbore while the bottom-hole pressure is continuously monitored. After a quasi-steady pressure state is reached, the injection is shut in abruptly and the pressure decline is recorded. For radial flow conditions, the permeability k can be derived from the slope of the semi-logarithmic plot of the pressure change versus the Horner time factor during the pressure-falloff period. The corresponding formula is

$$k = \frac{171.5q\mu}{mh} \tag{4}$$

where q is the injection rate (m^3·day^{-1}), μ is the viscosity of the injected fluid (mPa·s), h is the effective coal seam thickness (m), and m is the slope (Pa per logarithmic cycle) obtained from the straight-line portion of the semi-log plot. For each test, we used the recorded injection rate and water viscosity (≈1.0 mPa·s at reservoir temperature) along with the effective thickness of the seam to calculate the permeability. This methodology follows standard CBM well test interpretation practice.

3.2. Microseismic Monitoring of Hydraulic Fracturing Fractures

Microseismic monitoring during hydraulic fracturing is essential for characterizing the nature and spatial behavior of induced reservoir fractures. Microseismic signals induced by coal-seam hydraulic fracturing are detected, identified, and processed using automated weak-event recognition techniques. The recorded microseismic data are then further analyzed using high-precision event-location algorithms. This enables the determination of key parameters such as the spatial coordinates and origin time of fractures induced within the coal–rock mass by hydraulic fracturing.

In this study, microseismic fracture monitoring was performed with 12 three-component borehole/surface sensors deployed in an annular array around the target wells. The system sampled at 1 ms and recorded continuously for 195 min during stimulation and early shut-in. Real-time data transmission was employed to enable a rapid on-site response and quality control during fracturing operations. Event locations were determined using a forward-modeling grid-search algorithm followed by a secondary fine-grid search to refine the source positions. These procedures allow for the automated identification and location of microseismic events while minimizing subjective intervention. Additionally, time-shift and stacking concepts commonly used in conventional seismic processing were incorporated into the workflow. A locally calibrated velocity model constructed from borehole acoustic logs was preferentially employed. This approach enhanced both the reliability of the event-location results and the computational efficiency. Source dimension parameters were estimated using Brune's spectral model together with the Madariaga half-period method to obtain the source radius [20].

Finally, the uncertainties associated with the fracture length and height were assessed using error-propagation equations combined with a normal-distribution analysis. In this study, uncertainties in the sampling interval, travel time, and velocity were considered the primary contributors to the overall error. A T-test at a 75% confidence level was then applied to derive confidence intervals for the fracture-geometry parameters.

4. Results

4.1. In Situ Stress

The following sections analyze in situ stress data obtained from the hydraulic fracturing method with multi-cycle injection tests in 13 coalbed methane wells in the Yangquan mining area.

4.1.1. Characteristics of In Situ Stress and Its Vertical Zonation

With increasing burial depth, both the in situ stress and reservoir pressure in the study area exhibited an increasing trend, with different variation patterns at different depths (Figure 4). This may have been influenced by tectonic movements and geological conditions [12]. The minimum horizontal principal stress (σ_h) ranged from 3.72 to 13.24 MPa, with an average value of 8.64 MPa. The maximum horizontal principal stress (σ_H) ranged from 4.04 to 23.41 MPa, with an average value of 14.54 MPa. The vertical stress (σ_v) ranged from 6.5 to 19.87 MPa, with an average value of 13.31 MPa. The reservoir pressure ranged from 0.55 to 6.09 MPa, with an average value of 2.32 MPa. According to the four-level in situ stress classification criteria for coal reservoirs established based on the magnitude of the minimum horizontal principal stress, which was proposed by Kang et al. [21], coal reservoirs can be divided into four grades: the ultra-low-stress zone ($\sigma_h < 10$ MPa), medium-stress zone (10 MPa $\leq \sigma_h <$ 18 MPa), high-stress zone (18 MPa $\leq \sigma_h <$ 30 MPa), and ultra-high-stress zone ($\sigma_h \geq 30$ MPa). In the Yangquan Mining Area, the minimum horizontal principal stress ranged from 3.72 to 13.24 MPa, with an average value of 8.64 MPa. Therefore, most measurement points fell within the low- to medium-stress

ranges. Overall, the study area can be characterized as a predominantly low-stress area with local medium-stress anomalies, and the in situ stress magnitude generally decreases upward with decreasing burial depth.

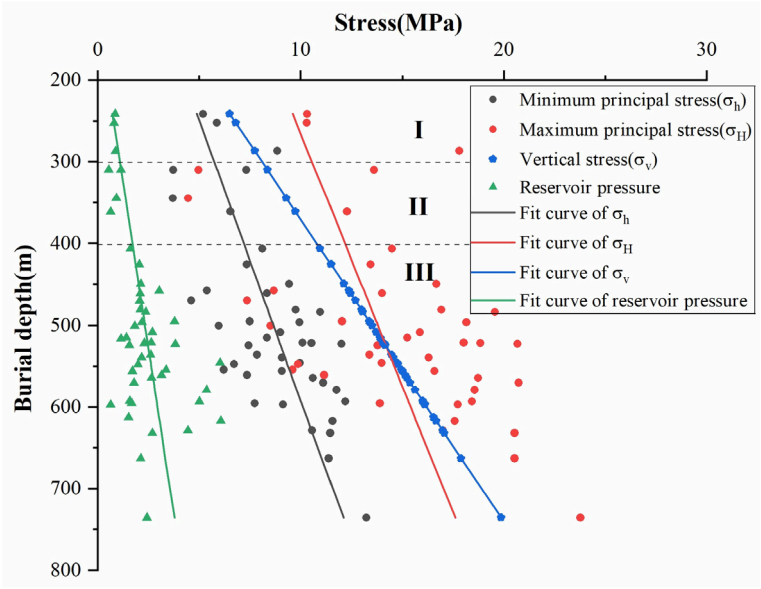

Figure 4. Variation in in situ stresses and reservoir pressure with burial depth.

Anderson's faulting theory posits three stress regimes that can be used to describe the in situ stress states [22,23]:

1. The stress regime of normal faulting: The vertical stress is the maximum principal stress, with $\sigma_v > \sigma_H > \sigma_h$. In this case, normal faulting is driven by gravity or vertical stress, and fault slide happens when the minimum stress drops to a low-enough level.
2. The stress regime of strike-slip faulting: The vertical stress is the intermediate principal stress. In this stress state, one has $\sigma_H > \sigma_v > \sigma_h$.
3. The stress regime of reverse (or thrust) faulting. The vertical stress is the least principal stress, with $\sigma_H > \sigma_h > \sigma_v$.

According to Anderson's faulting theory and the relationship between σ_h, σ_H, and σ_v in the study area, three types of stress fields can be identified along the depth profile.

(I) For the coal reservoirs with a burial depth shallower than 300 m, the in situ stress state principally shows the type of $\sigma_H > \sigma_v > \sigma_h$, of which the horizontal principal stress is dominant. In this depth range, the σ_h (5.19–8.86 MPa, average of 6.64 MPa) and the σ_H (10.30–17.21 MPa, average of 12.61 MPa) increase following a linear relationship as the coal seam burial depth increases.

(II) In the coal reservoir at depths ranging from 300 to 400 m, as the depth increases, the σ_v (8.36–9.75 MPa, average of 8.94 MPa) becomes greater than the σ_H (4.04–11.9 MPa, average of 8.325 MPa), whereas the σ_h remains consistently lower than the σ_v. Given the limited number of data points in this depth range, it was tentatively concluded that the in situ stress state follows the pattern of $\sigma_v > \sigma_H > \sigma_h$, with the stress regime being classified as a normal fault stress regime and the current stress state being extensional.

(III) A total of 34 samples were collected from the coal reservoir at depths between 400 and 800 m. Inspection of the trend lines revealed that they converge around a burial depth of approximately 550 m, at which point the maximum horizontal principal stress and the vertical principal stress become comparable. At some deeper measurement points, the vertical stress even exceeds the maximum horizontal stress ($\sigma_v > \sigma_H$). Among these,

67.9% of the sample points exhibit $\sigma_H > \sigma_v > \sigma_h$, while 32.1% show $\sigma_v > \sigma_H > \sigma_h$. The stress regime associated with strike-slip faults again predominates.

In general, the regional stress field was dominated by a strike-slip faulting regime with $\sigma_H > \sigma_v > \sigma_h$, accounting for 23 measurement points. The present stress state is compressive. In coal seams 8# and 9#, a normal faulting regime ($\sigma_v > \sigma_H > \sigma_h$) was observed at some measurement points, totaling 11 points, and the current stress state was extensional.

4.1.2. Relationship of Vertical Stress and Horizontal Stresses

The relationship between horizontal stresses and the overburden stress can be examined using the lateral stress coefficient (λ), which is defined as the ratio of the average horizontal principal stress, $(\sigma_h + \sigma_H)/2$, to the vertical stress, σ_v [18,22]. The spatial distribution of λ significantly influences the permeability of coal reservoirs and governs hydraulic-fracture propagation. The vertical strength coefficient N is a key parameter characterizing the relationship between vertical stress and the uniaxial compressive strength of coal and rock; it is used to assess the degree of vertical stress concentration in the reservoir and potential failure modes.

$$\lambda = \frac{(\sigma_h + \sigma_H)/2}{\sigma_v} \tag{5}$$

$$N = \frac{\sigma_h}{\sigma_v} \tag{6}$$

The measured lateral stress coefficient λ ranged from 0.45 to 1.68, with an average value of 0.89. Approximately 97% of the data points fell within the in situ stress envelopes reported for mainland China [24,25] (Figure 5). By fitting the trend line to the relationship between the burial depth and λ, it was observed that the λ of the in situ stress field decreased with increasing burial depth, exhibiting characteristics of "shallow dispersion and deep convergence", and the empirical formula was derived:

$$\lambda = \frac{189.22}{H} + 0.41 \tag{7}$$

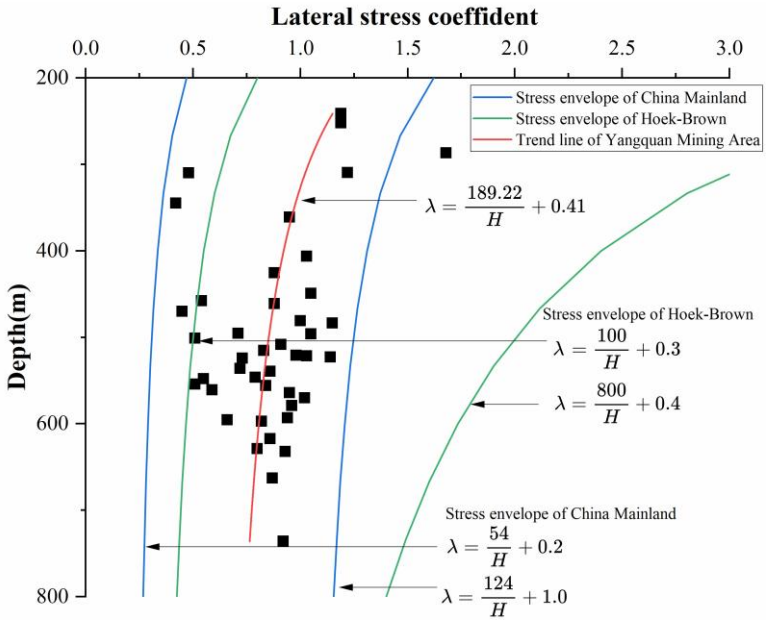

Figure 5. Depth-dependent variation in lateral stress coefficient (λ) in study area.

The data indicate that the λ of the in situ stress field decreased with increasing burial depth, exhibiting a pattern of "dispersal in shallow areas and convergence in deeper areas". Certain points were outliers, potentially corresponding to localized extensional or compressive structures, stress concentration caused by faults, or stress-relief zones, all of which lead to stress anomalies.

4.2. Permeability

Permeability is a key parameter that influences the coalbed methane production performance. The primary factors affecting permeability in coal reservoirs are the pore structure and stress conditions [26,27]. In the study area, the coal seam permeability ranged from 0.03 to 15.52 mD, with an average value of 1.62 mD. The coal seams in this region generally exhibited a low permeability, with most well tests yielding values below 1 mD (Table 2). However, a few anomalous high-permeability points exceeded 10 mD, causing the permeability distribution to be significantly skewed and resulting in a high variance (Figure 6). To reduce the visual and statistical influence of these high-permeability outliers, the subsequent permeability-related plots were presented using a logarithmic permeability scale. This treatment is appropriate because permeability is a positive-valued parameter and commonly exhibits right-skewed or approximately log-normal behavior in reservoir studies.

Table 2. In situ stress characteristics of coal seams in the Yangquan mining area.

Well No.	Coal Number	Depth (m)	Minimum Horizontal Principal Stress (MPa)	Maximum Horizontal Principal Stress (MPa)	Reservoir Pressure (MPa)	Vertical Stress (MPa)	Lateral Stress Coefficient	Vertical Stress Coefficient	Permeability (mD)
KY01	3#	406.45	8.12	14.5	1.63	10.97	1.03	0.74	0.07
	9#	449.25	9.43	16.07	2.13	12.13	1.05	0.78	0.06
	15#	521.68	10.55	18.48	2.32	14.09	1.03	0.75	0.1
KY02	3#	252.20	5.88	10.3	0.82	6.81	1.19	0.86	3.96
	9#	309.68	7.32	13	1.16	8.36	1.22	0.88	0.39
KY03	3#	241.13	5.19	10.33	0.86	6.51	1.19	0.80	0.17
	9#	286.75	8.86	17.21	0.89	7.74	1.68	1.14	0.16
	15#	361.25	6.55	11.9	0.65	9.75	0.95	0.67	7.61
PS01	8#	309.95	3.72	4.36	0.55	8.37	0.48	0.44	12.3
PS02	8#	470.18	4.61	6.77	2.09	12.69	0.45	0.36	7.62
	15#	548.00	6.73	9.51	1.99	14.80	0.55	0.45	15.52
PS03	8#	515.20	8.35	14.64	1.42	13.91	0.83	0.60	1.29
	15#	597.30	9.14	17.37	0.65	16.13	0.82	0.57	11.71
PS04	6#	425.65	7.35	12.91	2.07	11.49	0.88	0.64	0.04
	8#	457.78	5.39	8.17	3.04	12.36	0.55	0.44	0.2
	15#	539.48	9.08	15.94	2.17	14.57	0.86	0.62	0.09
PS05	8#	483.75	10.97	18.95	2.38	13.06	1.15	0.84	0.13
	15#	564.30	10.62	18.38	2.67	15.24	0.95	0.70	0.73
PS06	8#	554.30	6.22	9.01	3.37	14.97	0.51	0.42	0.11
	15#	632.13	11.45	20.17	2.71	17.07	0.93	0.67	0.24
PL19	6#	461.30	8.35	13.5	2.1	12.46	0.88	0.67	0.05
	8#	481.03	9.77	16.3	2.11	12.99	1.00	0.75	0.13
	9#	501.10	5.98	7.92	1.85	13.53	0.51	0.44	0.05
	15#	570.28	11.12	20.36	1.79	15.40	1.02	0.72	0.13
QW12	8#	663.08	11.40	19.93	2.13	17.90	0.87	0.64	0.16
	15#	736.08	13.24	23.41	2.45	19.87	0.92	0.67	0.03
XS9	3#	508.58	9.01	15.88	2.71	13.73	0.91	0.66	0.89
	6#	536.10	7.86	12.87	2.62	14.47	0.72	0.54	0.22
	9#	561.02	7.38	10.57	3.16	15.15	0.59	0.49	3.36
	15#	628.80	10.57	16.64	4.46	16.98	0.80	0.62	0.06
XS43	3#	496.35	9.95	18.17	2.2	13.40	1.05	0.74	0.2
	6#	522.92	12.02	20.15	3.84	14.12	1.14	0.85	0.15
	9#	546.35	9.96	13.39	6.04	14.75	0.79	0.68	0.21
	15#	617.25	11.57	17.21	6.09	16.67	0.86	0.69	0.137

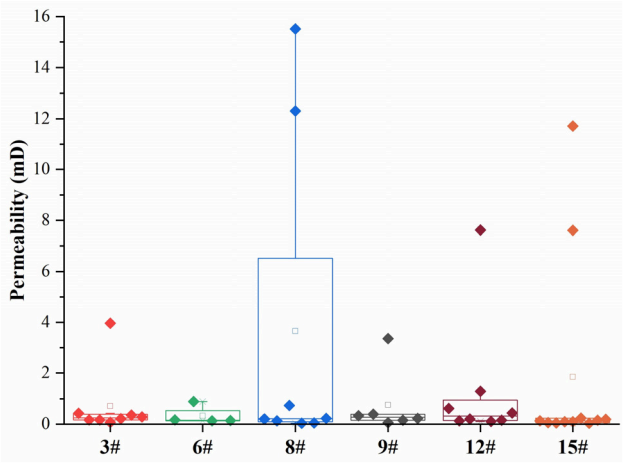

Figure 6. Distribution of coal-reservoir permeability across different coal seams in the study area.

Permeability varies significantly among coal seams. Based on Table 2, the 15# and 8# seams showed a relatively higher average permeability and larger fluctuations, with mean values of 3.31 mD and 2.74 mD, respectively, reflecting strong heterogeneity and several anomalous high-permeability intervals. In contrast, the 6# seam had the lowest average permeability and limited fluctuations, approximately 0.12 ± 0.09 mD, indicating that it is predominantly low-permeability and relatively uniform. Differences in permeability among coal seams may be influenced by the fracture connectivity, lithological variation, proximity to faults, and mechanical properties of the surrounding strata.

4.3. Hydraulic Fracture Morphology and Spatial Distribution Characteristics

Microseismic monitoring of 23 hydraulic fracture treatments in the study area indicated that the dominant hydraulic-fracture orientations were clustered between NE5° and NE55°, representing roughly 74% of all fracture observations. The fracture lengths varied from 124.9 to 447.7 m, yielding an average length of 344.7 m and a median of 390.8 m, indicating that the fracture lengths generally fell within the 10^2 m order of magnitude, with substantial spatial variability (Table 3). The fractures exhibited an overall near-vertical dip, characteristic of vertically oriented hydraulic fractures.

It should be noted that the hydraulic-fracturing treatments summarized in Table 3 were performed in several coal seams (3#, 8#, 9# and 15#) within the Carboniferous–Permian Shanxi and Taiyuan Formations. These seams belong to the same coal-bearing stratigraphic unit and therefore exhibit broadly similar lithological compositions and coal-quality parameters (see Table 1 for the seam thickness, vitrinite content and ash yield). This similarity allows us to examine macro-scale relationships between the in situ stress, permeability and fracture morphology across different burial depths. However, the depth intervals listed in Table 3 correspond to different seams (approximately 520–780 m), and the intensity of pre-existing natural fractures can vary with burial depth and local geological structures. Numerous laboratory and numerical studies indicate that natural fractures and bedding laminae markedly influence hydraulic-fracture propagation—fractures may initiate at the ends of natural fractures and evolve from nearly linear to echelon or network patterns as weak planes increase. Such micro-scale heterogeneity may cause individual fractures in shallow, highly fractured seams to deviate or branch from the maximum stress direction, whereas deeper seams with fewer open fractures favor longer, planar fractures. Because this study investigated the macro-scale relationships between the in situ stress and fracture orientation/length, the influence of individual natural fractures was considered minor for our study.

Table 3. Microseismic monitoring statistics of hydraulic-fracturing treatments in the Yangquan mining area.

Well No.	Depth (m)	Azimuth (°)	Fracture Length (m)	Fracture Length of West Wing (m)	Fracture Length of East Wing (m)	Fracture Height (m)	Inclination (°)	Morphology
X-4	632	NE78	438.2	206.7	231.5	40	2	Vertical
XJ-42	737	NE13	440.7	208.1	232.6	40.56	3	Vertical
XJ-46	756	NE30	442.9	211.9	231	39.31	4	Vertical
XJ-50	780	NE28	440.4	210.9	229.5	40.67	4	Vertical
XY-6	/	NE50	378.9	182.7	196.2	28.5	1	Vertical
XY-8	613	NE15	423.2	192.7	230.5	28.5	1	Vertical
XY-4	/	NS	390.8	185.6	205.2	28.5	1	Vertical
XY-10	627	NE52	447.7	214.1	233.6	28.5	1	Vertical
XW-1	645	NE30	424.2	210.3	213.9	23.3	2	Vertical
XW-2	612	NE32	420.3	191.7	228.6	24.2	2	Vertical
XW-3	572	NE63	447.3	214.7	232.6	16.3	4	Vertical
XW-4	549	NE48	443.4	211.5	231.9	27.4	1	Vertical
XW-5	526.3	NE63	445.3	213.8	231.5	12.9	4	Vertical
PSW-4	545	NE4	189.4	/	/	45.13	/	Vertical
PSW-6	520	NS	206.6	/	/	63.46	/	Vertical
PSW-5	520	NE6	282.2	/	/	56.12	/	Vertical
PSW-1	573	NW22	124.9	/	/	36.66	/	Vertical
X-14	615.3	NE29	189.8	/	/	68.31	/	Vertical
X-3	635.1	NE19	282.9	/	/	79.09	/	Vertical
X-2	675.1	NE12	263.5	/	/	70.02	/	Vertical
XY-25	561.25	NW	224.4	/	/	62.56	/	Vertical
XY-24	554.85	NW	288.9	/	/	69.33	/	Vertical
XY-23	590.75	NW	292.0	/	/	59.6	/	Vertical

The statistical analysis of dominant microseismic fracture orientations showed that NNE-oriented fractures represent the largest group in the study area, with nine occurrences; this was followed by NS-oriented fractures, with four samples, and NE–ENE orientations, with a total of six samples (Figure 7). The fracture lengths were classified according to the dominant fracture orientation, and fractures generated in different directions showed significant differences in extension length, with NNE-, NE-, and ENE-oriented fractures demonstrating substantially greater extension magnitudes, supporting the conclusion that preferred fracture orientations exhibit advantages both in directional dominance and in extension scale (Figure 8).

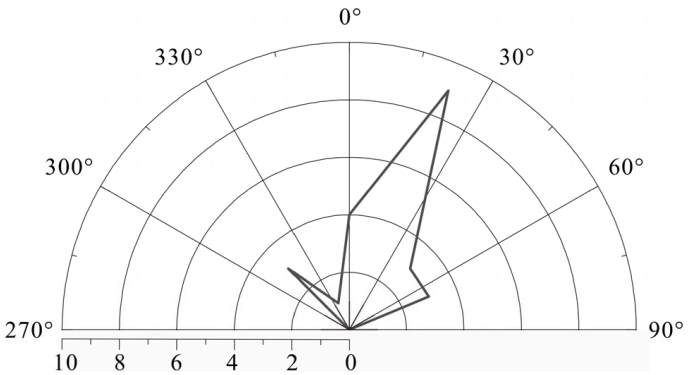

Figure 7. Rose diagram of hydraulic fracture orientations derived from microseismic fracture monitoring in the study area.

In summary, hydraulic fractures in the study area predominantly trended NNE, and these preferred orientations exhibited significantly greater extension lengths. The observed fracture orientations were aligned with the regional maximum horizontal principal stress direction, indicating that the in situ stress field serves as the primary control on both the preferred fracture orientation and fracture-extension magnitude.

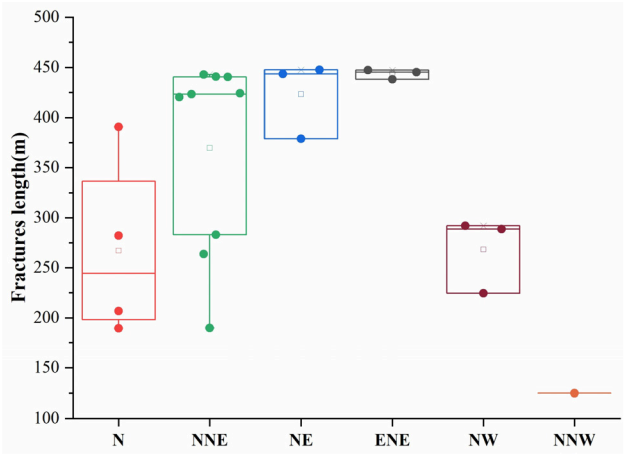

Figure 8. Relationship between hydraulic fracture length and dominant fracture orientation in the study area.

5. Discussion

5.1. Influence of Coal Thickness on Permeability

An analysis of the relationship between the coal seam thickness and the well-test permeability showed that permeability behaviors bifurcate at approximately 1 mD, with coal thickness exerting a distinctly segmented control (Figure 9). In low-permeability reservoirs (k < 1 mD), the permeability decreased with increasing coal thickness, indicating a negative correlation. In contrast, in high-permeability intervals (k > 1 mD), the permeability increased with coal thickness, displaying a clear positive correlation.

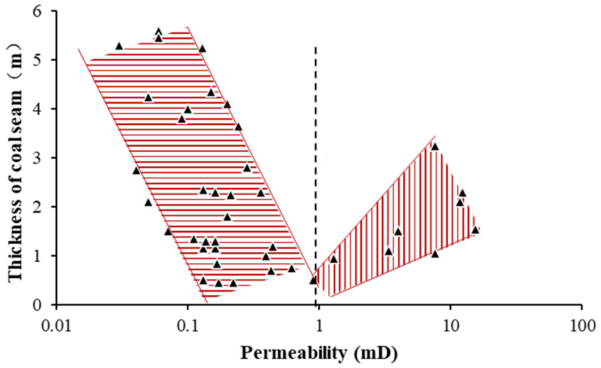

Figure 9. Segmented relationship between coal-reservoir permeability and coal seam thickness.

The dual behavior between the coal seam thickness and permeability should not be interpreted as a simple single-factor control of coal thickness. Instead, it reflects the combined influence of coal seam thickness, natural fracture development, in situ stress conditions, and coal-seam heterogeneity. In coal reservoirs, permeability is mainly controlled by the aperture, density, and connectivity of cleats and tectonic fractures. Therefore, the same increase in coal seam thickness may produce different permeability responses under different fracture-development and stress conditions.

For the low-permeability group (k < 1 mD), the permeability decreased with increasing coal seam thickness. This negative correlation indicates that these samples were mainly governed by a stress-closure-dominated regime. In this regime, thicker coal seams do not necessarily contain more effective flow channels. On the contrary, under an increasing burial depth and horizontal compression, natural fractures and cleats tend to close, and the effective fracture density and connectivity may decrease. In addition, thicker coal intervals may contain more strongly compacted or poorly connected coal layers, which reduces the

contribution of individual fractures to the overall flow capacity. As a result, the measured permeability remains low and may decrease with increasing coal seam thickness.

In contrast, for the high-permeability group (k > 1 mD), the permeability increased with coal seam thickness, suggesting a fracture-connectivity-dominated regime. These high-permeability intervals are likely associated with well-developed natural fractures, locally favorable structural conditions, or interbedded sandstone lenses that improve the connectivity of the flow system. Under such conditions, a thicker coal seam can provide a larger effective flow interval and a greater probability of intersecting connected cleat–fracture networks. Therefore, the permeability increases with coal seam thickness in the high-permeability domain.

Accordingly, the apparent dual behavior shown in Figure 9 reflects a transition between two different permeability-control mechanisms. In the low-permeability domain, the permeability was mainly limited by in situ stress-induced fracture closure and poor fracture connectivity. In the high-permeability domain, the permeability was mainly enhanced by the development and preservation of connected natural fractures. This segmented relationship further indicates that the coal seam thickness alone cannot fully determine the reservoir permeability; instead, its effect must be evaluated together with the in situ stress, fracture development, lithological variation, and local structural conditions.

5.2. Influence of In Situ Stress on Permeability

A statistical analysis of 13 well-test samples from the Yangquan mining area revealed a pronounced negative correlation between burial depth and permeability. The depth-dependent behavior of permeability in the study area can be summarized as follows: In the shallow section, the permeability increased initially and then decreased, reaching a local maximum at approximately 300 m. This depth interval coincided with a transition in the stress regime from a strike-slip faulting stress regime ($\sigma_H > \sigma_v > \sigma_h$) to a normal faulting stress regime ($\sigma_v > \sigma_H > \sigma_h$) (Figure 10). Over this transition, the horizontal stress decreased slightly, whereas the vertical stress progressively became the dominant component. As a result, the coal reservoir experienced a relatively tensile stress condition, leading to increasing permeability with depth. With continued burial, horizontal stresses regained dominance, causing the stress regime to shift back to a strike-slip type [28]. Under increasing horizontal compression, pores and fractures progressively closed, resulting in a decline in permeability with increasing depth. However, an abnormally high permeability point appeared near 500 m. This anomalous point was associated with the No. 8 coal seam. It was inferred that locally developed natural fractures or interbedded sandstone lenses created highly connected flow pathways [29]. Additionally, reduced local confining pressure may promote fracture preservation, collectively leading to an anomalously elevated permeability. The depth-dependent inflection points in permeability generally coincide with the depths at which stress-regime transitions occur. Therefore, the vertical permeability variations are fundamentally governed by the stress-regime type and its vertical partitioning [30].

Laboratory measurements indicated a strong correlation between the well-test permeability and in situ stress. The coal-reservoir permeability exhibited an exponential decline as the in situ stress increased [31,32]. The stress-dependent permeability of CBM reservoirs can be expressed by an exponential function:

$$K = K_0 e^{-a\sigma_e} \tag{8}$$

where K is the permeability (mD) and σ_e is the effective in situ stress (MPa). K_0 is the permeability under the initial in situ stress condition (mD) and a is the fitting parameter depending on the type of principal stress.

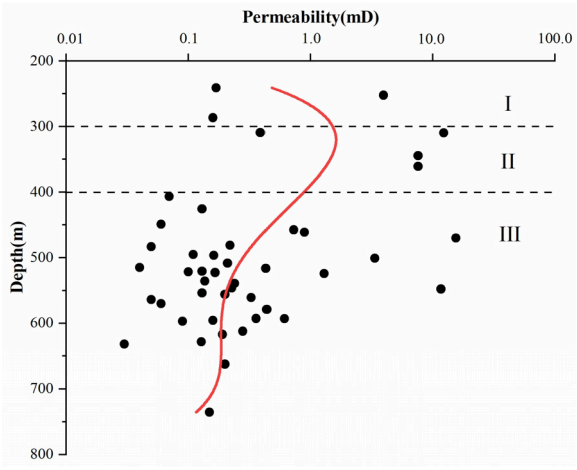

Figure 10. Relationship between coal-reservoir permeability and burial depth in study area.

In the study area, the coal-reservoir permeability decreased markedly as both the horizontal principal stresses and their differential increased (Figures 11–13). The measured permeability of CBM reservoirs in the study area exhibited approximate exponential relationships with the maximum horizontal stress, minimum horizontal stress, and horizontal stress difference. These relationships are consistent with established empirical formulations:

$$K = 11.771\mathrm{e}^{-0.254\sigma_H} \quad (9)$$

$$K = 12.379\mathrm{e}^{-0.43\sigma_h} \quad (10)$$

$$K = 5.2196\mathrm{e}^{-0.495(\sigma_H-\sigma_h)} \quad (11)$$

where K is the permeability (mD) and σ_H and σ_h are the principal maximum horizontal and minimum horizontal stresses (MPa).

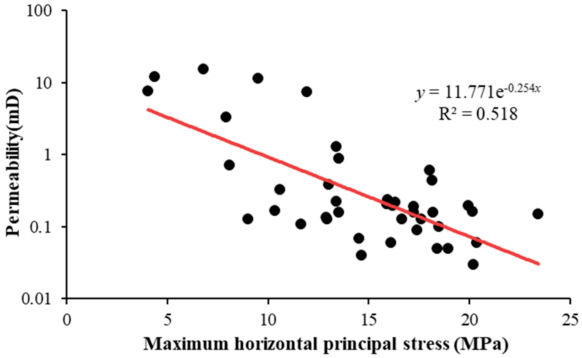

Figure 11. Relationship between permeability and maximum horizontal principal stress.

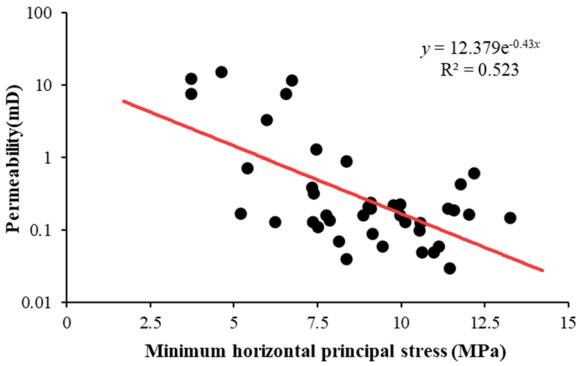

Figure 12. Relationship between permeability and minimum horizontal principal stress.

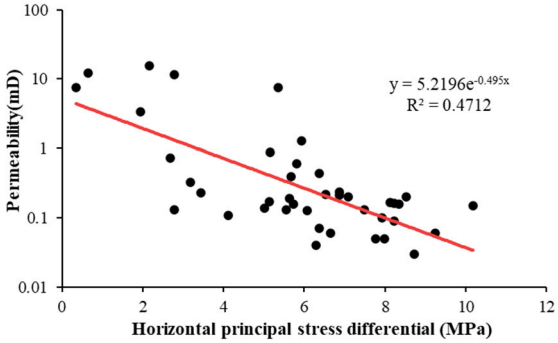

Figure 13. Relationship between permeability and horizontal principal stress differential.

As the horizontal principal stresses increased, pores and fractures within the coal reservoir underwent compression, resulting in a reduced permeability. The differential between the horizontal principal stresses reflects the degree of stress anisotropy. This anisotropy controls the effective normal stress and shear stress acting on fracture surfaces. Consequently, it regulates the fracture aperture, slip behavior, and connectivity, collectively governing permeability variations. Therefore, the in situ stress field constitutes one of the primary geological controls on permeability. The results of this study show that coal-seam permeability decreases exponentially with increasing horizontal principal stresses and the horizontal principal stress difference. This finding is consistent with previous studies, which have demonstrated that in situ stress and stress-dependent fracture closure exert significant control on coal permeability and should be considered in CBM development and mine methane drainage/degassing designs [5,30,33]. Therefore, the study is quantitatively verified here for the Yangquan Mining Area. The regional exponential regression models and fitting coefficients obtained in Equations (9)–(11) provide site-specific quantitative references for identifying favorable permeability intervals and optimizing methane drainage/degassing and hydraulic-fracturing designs in deep coal seams of the Yangquan Mining Area.

5.3. Influence of In Situ Stress on Hydraulic Fracture Morphology

Microseismic events obtained during hydraulic fracturing were processed and spatially located to reconstruct the three-dimensional fracture network (Figure 14). In Figure 14, different colors are used to denote the main hydraulic fracture orientations. For Well XJ-42, the main fracture (purple-red) trended NE13° and was accompanied by three subsidiary branches. The main fracture in Well XJ-46 (red) trended NE30° and contained four secondary branches. The main fracture associated with Well XJ-50 (purple-red) trended NE28° and included two branch fractures. For Well XY-4, the main fracture (blue) was oriented approximately north–south and exhibited four subsidiary branches. The main fracture in Well XY-6 (blue) trended NE50° and contained four branch fractures. The main fracture in Well XY-8 (blue) trended NE15° and was associated with three branch fractures. These observations show that the preferred fracture orientations coincide with the regional stress field in the Yangquan area, predominantly trending NNE–NE. The fracture lengths generally fell within the hundred-meter to several-hundred-meter scale, exhibiting a greater propagation extent and stronger directional clustering along the dominant orientations. This pattern indicates that the regional maximum horizontal principal stress governs both the preferred fracture orientation and the extent of fracture propagation. This occurs because fractures preferentially dilate in the direction of the maximum horizontal principal stress in a three-dimensional stress regime [34]. In this direction, the combination of effective stresses and shear stresses acting on fracture planes is most favorable for fracture dilation and propagation.

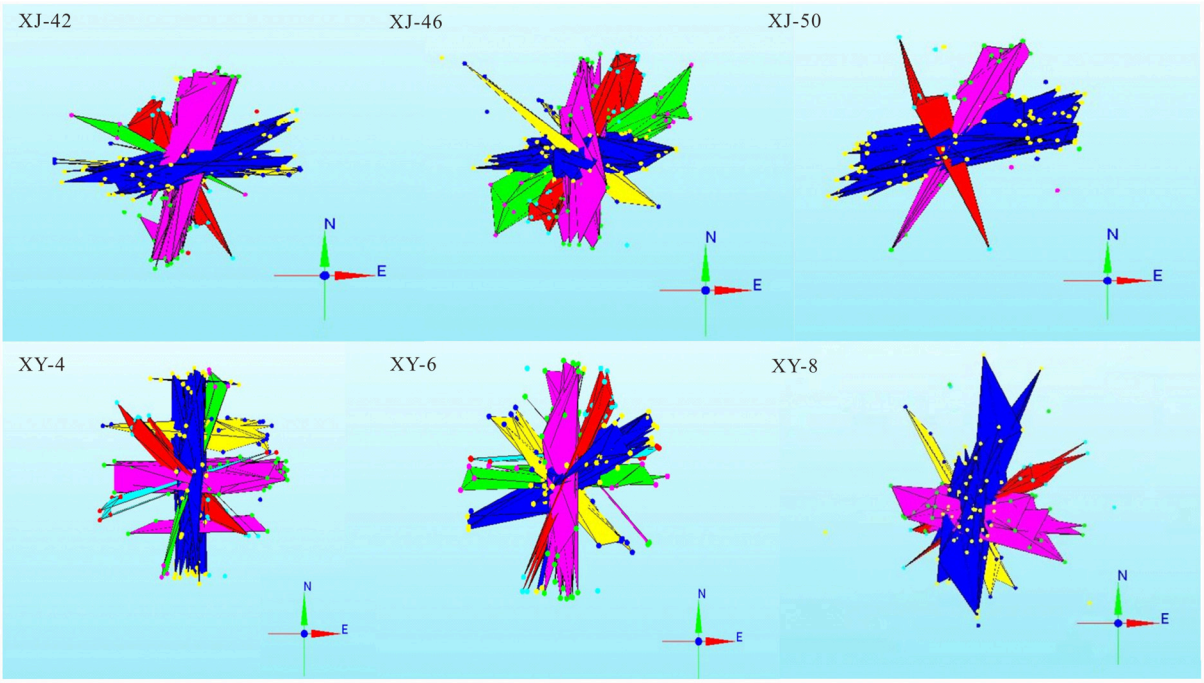

Figure 14. Three-dimensional fracture network reconstructed from microseismic monitoring in study area.

Given the relatively low tensile strength of the coal–rock matrix in both principal directions, with the difference typically smaller than 0.5 MPa, the fracture orientation was dictated by the prevailing in situ stress regime rather than material anisotropy. In both Zone I and Zone II, the vertical stress exceeded the minimum horizontal principal stress, indicating that the minimum principal stress remained horizontal. According to fracture mechanics principles, hydraulic fractures propagate perpendicular to the minimum principal stress; consequently, fracturing in both zones predominantly generated vertical fractures. This mechanical interpretation is consistent with the microseismic fracture monitoring results.

The horizontal principal stress differential is a key parameter governing the fracture propagation orientation, geometric configuration, and overall extension during hydraulic fracturing [35]. Because fractures propagate perpendicular to the minimum principal stress, increasing the stress differential intensifies stress anisotropy and concentrates deformation along the direction of the maximum horizontal principal stress. This enhanced anisotropy suppresses fracture branching and promotes the formation of a single, planar fracture system instead of a complex fracture network.

An integrated analysis of the fracture length and horizontal principal stress differential revealed a strong positive correlation within the study area (Figure 15). The fracture length increased systematically with increasing stress differential. Under a low horizontal stress differential, fractures tended to undergo shear reactivation and develop complex branching, resulting in diffuse or feather-like fracture geometries [36,37]. In contrast, a high horizontal stress differential suppressed branching and deviation, promoting the formation of single, planar fractures aligned with the maximum horizontal principal stress. This behavior can be attributed to the fact that increasing the horizontal principal stress differential enhances the fracture's ability to penetrate interlayers while restricting fracture height growth, thereby promoting lateral propagation. Furthermore, a greater stress differential intensifies stress concentration at the fracture tip and reduces propagation resistance along the maximum horizontal principal stress direction, resulting in longer dominant fractures. These findings indicate that optimizing the coupling between the in situ stress differential and engineering

parameters can effectively regulate the fracture trajectory and extension, thereby improving the stimulation efficiency of coal reservoirs.

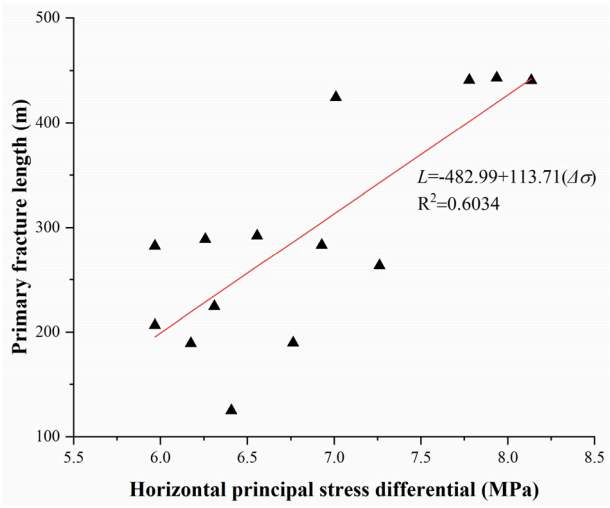

Figure 15. Relationship between primary fracture length and horizontal principal stress differential in study area.

However, this pattern is not absolute in reservoirs with strong anisotropy, pronounced bedding, or a high density of natural fractures. Recent acoustic-emission and CT imaging experiments showed that, as the horizontal stress differential increases from 4 MPa to 8 MPa, fractures can propagate across bedding planes toward the vertical direction, and the stimulation efficiency improves; the injection rate and fluid viscosity exert a decisive influence on the number of fractures and the degree of branching. Under lower stress differentials, more fractures are generated, but their height is restricted; under higher stress differentials, fractures tend to be singular, yet with appropriate injection parameters, a multi-branch network can still form [38]. In addition, numerical simulations indicate that excessively high stress differentials increase the initiation resistance of natural fractures and cause hydraulic fractures to propagate along the maximum principal stress direction; when the stress differential is around 4 MPa, the ratio of the fracture length to width is optimal, the fracture network is more complex, and the drainage efficiency is the highest [39]. Therefore, in anisotropic reservoirs, the inhibitory effect of high stress differentials on branching may be mitigated by the combined influence of bedding weaknesses and engineering parameters, and selecting a moderate stress differential and optimizing injection parameters are conducive to the formation of complex fracture networks.

6. Conclusions

This study integrated injection/falloff well-test data, coal-reservoir permeability measurements and microseismic monitoring to evaluate the stress-controlled permeability and hydraulic fracture behavior in the Yangquan Mining Area. The main conclusions are as follows:

1. Both in situ stress and reservoir pressure increased systematically with burial depth. Three vertical stress regimes were identified, and the overall regional stress field was dominated by strike-slip faulting ($\sigma_H > \sigma_v > \sigma_h$), implying a strong horizontal stress anisotropy throughout most of the coal-bearing section.
2. The coal-seam permeability ranged from 0.03 to 15.52 mD (average of 1.62 mD) and exhibited a segmented response to the coal-seam thickness. The permeability decreased exponentially with increasing effective stress, confirming that in situ stress is the primary geological control on CBM reservoir permeability. Depth-related

inflection points in the permeability corresponded to transitions between different stress regimes.

3. Microseismic monitoring of 23 hydraulic fracturing treatments showed that induced fractures trended predominantly NNE–NE and were vertical. The fracture length and morphology were strongly dependent on the horizontal principal stress differential: larger stress differentials suppressed branching and promoted the formation of longer, planar fractures oriented perpendicular to σh, whereas smaller differentials favored branching and the development of complex fracture networks.
4. These findings demonstrate the critical role of the in situ stress field in governing both the coal-reservoir permeability and hydraulic fracture morphology. By integrating stress regime characteristics with coal-seam properties, this study provides a scientific basis for well placement, stimulation designs and optimized CBM development in low- to medium-stress, multi-seam reservoirs such as the Yangquan Mining Area.

Author Contributions: B.M.: Writing—Original Draft Preparation; X.Z. and D.L.: Conceptualization, Writing—Reviewing and Editing; M.L. and X.D.: Formal Analysis; J.Z.: Writing—Reviewing and Editing; H.W.: Methodology; D.W.: Writing—Reviewing and Editing. All authors have read and agreed to the published version of the manuscript.

Funding: Funding was provided by the Youth Innovation Team Development Program of Shandong Province, China (2022KJ215), and the Open Competition Project of the China Coal First Geological Bureau Group Co., Ltd. (ZMYJ-JBGS-2025-02).

Data Availability Statement: The original contributions presented in this study are included in the article. Further inquiries can be directed to the corresponding authors.

Conflicts of Interest: The authors declare no conflicts of interest.

References

1. Karacan, C.Ö.; Ruiz, F.A.; Cote, M.; Phipps, S. Coal mine methane: A review of capture and utilization practices with benefits to mining safety and to greenhouse gas reduction. *Int. J. Coal Geol.* **2011**, *86*, 121–156. [CrossRef]
2. Li, P.; Zhang, X.; Li, J.; Zhao, J.; Huang, J.; Zhang, S.; Zhou, S. Analysis of the key factors affecting the productivity of coalbed methane wells: A case study of a high-rank coal reservoir in the central and southern Qinshui Basin, China. *ACS Omega* **2020**, *5*, 28012–28026. [CrossRef]
3. Zoback, M.L.; Zoback, M.D.; Adams, J.; Assumpcao, M.; Bell, S.; Bergman, E.A.; Blümling, P.; Brereton, N.R.; Denham, D.; Ding, J.; et al. Global patterns of tectonic stress. *Nature* **1989**, *341*, 291–298. [CrossRef]
4. Gao, Q.; Liu, J.; Huang, Y.; Li, W.; Shi, R.; Leong, Y.-K.; Elsworth, D. A critical review of coal permeability models. *Fuel* **2022**, *326*, 125124. [CrossRef]
5. Meng, Z.; Zhang, J.; Wang, R. In-situ stress, pore pressure and stress-dependent permeability in the Southern Qinshui Basin. *Int. J. Rock Mech. Min. Sci.* **2011**, *48*, 122–131. [CrossRef]
6. Tiab, D.; Donaldson, E.C. *Petrophysics: Theory and Practice of Measuring Reservoir Rock and Fluid Transport Properties*, 2nd ed.; Gulf Professional Publishing: Houston, TX, USA, 2004.
7. Palmer, I.; Mansoori, J. How permeability depends on stress and pore pressure in coalbeds: A new model. *SPE Reserv. Eval. Eng.* **1998**, *1*, 539–544. [CrossRef]
8. Ren, Q.; Zhang, C.; Wu, G.; Zhang, H.; Gao, S.; Sun, Z.; Gao, Y. Hydraulic fracture initiation and propagation in deep coalbed methane reservoirs considering weak plane: CT scan testing. *J. Nat. Gas Sci. Eng.* **2024**, *125*, 205286. [CrossRef]
9. Shi, X.; Yang, Y.-Y.; Kong, X.-W.; Gao, Q.; Jiang, S.; Mao, H.-J. Experimental study of hydraulic fracture propagation with multi-cluster in-plane perforations in a horizontal well. *Pet. Sci.* **2024**, *21*, 3258–3270. [CrossRef]
10. Lakirouhani, A.; Jolfaei, S. Assessment of hydraulic fracture initiation pressure using fracture mechanics criterion and coupled criterion with emphasis on the size effect. *Arab. J. Sci. Eng.* **2024**, *49*, 5897–5908. [CrossRef]
11. Li, R.; Zhang, L.; Xie, J.; Chen, Z.; Yang, B.; Xiang, W.; Zhai, X. A study on the controlling effect of geological structures on coalbed methane occurrence in the northeast margin of Qinshui Basin, North China. *Energies* **2025**, *18*, 647. [CrossRef]
12. Cao, T.; Yang, Z.; Qin, Y.; Yan, Z.; Chen, Z.; Li, C. Characteristics of modern geostress and removability of No. 15 coal reservoir, Yangquan Mining Area, China. *Nat. Resour. Res.* **2021**, *30*, 2211–2223. [CrossRef]

13. Hu, G.; Xu, J.; Zhang, F.; Zhao, C.; Qin, W.; Zhu, Y. Coal and Coalbed Methane Co-Extraction Technology Based on the Ground Movement in the Yangquan Coalfield, China. *Energies* **2015**, *8*, 6881–6897. [CrossRef]
14. Zhou, F.; Yao, G. Sensitivity analysis in permeability estimation using logging and injection-falloff test data for an anthracite coalbed methane reservoir in Southeast Qinshui Basin, China. *Int. J. Coal Geol.* **2014**, *131*, 41–51. [CrossRef]
15. Yang, Y.; Sun, D.; Ma, X.; Wu, B.; Chen, Q. A total system stiffness approach for determining shut-in pressure in hydraulic fracturing stress measurements. *Int. J. Rock Mech. Min. Sci.* **2025**, *192*, 106160. [CrossRef]
16. Liu, G.; Ehlig-Economides, C. Practical considerations for diagnostic fracture injection test (DFIT) analysis. *J. Pet. Sci. Eng.* **2018**, *171*, 1133–1140. [CrossRef]
17. Hubbert, M.K.; Willis, D.G. Mechanics of hydraulic fracturing. *Trans. AIME* **1957**, *210*, 153–168. [CrossRef]
18. Haimson, B.; Fairhurst, C. Initiation and extension of hydraulic fractures in rocks. *Soc. Pet. Eng. J.* **1967**, *7*, 310–318. [CrossRef]
19. Brown, E.T.; Hoek, E. Trends in relationships between measured in-situ stresses and depth. *Int. J. Rock Mech. Min. Sci. Geomech. Abstr.* **1978**, *15*, 211–215. [CrossRef]
20. Brune, J.N. Tectonic stress and the spectra of seismic shear waves from earthquakes. *J. Geophys. Res.* **1970**, *75*, 4997–5009. [CrossRef]
21. Kang, H.; Zhang, X.; Si, L.; Wu, Y.; Gao, F. In-situ stress measurements and stress distribution characteristics in underground coal mines in China. *Eng. Geol.* **2010**, *116*, 333–345. [CrossRef]
22. Anderson, E.M. The dynamics of faulting and dyke formation with applications to Britain. *Nature* **1942**, *149*, 651–652. [CrossRef]
23. Heidbach, O.; Rajabi, M.; Cui, X.; Fuchs, K.; Müller, B.; Reinecker, J.; Reiter, K.; Tingay, M.; Wenzel, F.; Xie, F.; et al. The World Stress Map database release 2016: Crustal stress pattern across scales. *Tectonophysics* **2018**, *744*, 484–498. [CrossRef]
24. Brown, E.T.; Hoek, E. *Underground Excavations in Rock*; CRC Press: Boca Raton, FL, USA, 1980.
25. Zhao, D.; Chen, Z.; Cai, X.; Li, S. Analysis of distribution rule of geostress in China. *Chin. J. Rock Mech. Eng.* **2007**, *26*, 1265–1271. (In Chinese)
26. Pan, Z.; Connell, L.D. Modelling permeability for coal reservoirs: A review of analytical models and testing data. *Int. J. Coal Geol.* **2012**, *92*, 1–44. [CrossRef]
27. Zhao, J.; Tang, D.; Xu, H.; Meng, Y.; Lv, Y.; Tao, S. A dynamic prediction model for gas-water effective permeability in unsaturated coalbed methane reservoirs based on production data. *J. Nat. Gas Sci. Eng.* **2014**, *21*, 496–506. [CrossRef]
28. Xu, H.; Tang, D.; Liu, D.; Tang, S.; Yang, F.; Chen, X.; He, W.; Deng, C. Study on coalbed methane accumulation characteristics and favorable areas in the Binchang area, southwestern Ordos Basin, China. *Int. J. Coal Geol.* **2012**, *95*, 1–11. [CrossRef]
29. Kang, Y.; Jiang, S.; Deng, Z.; Ma, Y.Z.; Wang, J.; Gu, J.; Sun, H. Non-monotonic decrease of coal permeability with depth in highly compressional tectonic settings: A case study in the Bide-Santang Basin, SW China. *Mar. Pet. Geol.* **2020**, *116*, 104321. [CrossRef]
30. Chen, S.; Tang, D.; Tao, S.; Xu, H.; Li, S.; Zhao, J.; Ren, P.; Fu, H. In-situ stress measurements and stress distribution characteristics of coal reservoirs in major coalfields in China: Implication for coalbed methane (CBM) development. *Int. J. Coal Geol.* **2017**, *182*, 66–84. [CrossRef]
31. Liu, Z.; Liu, D.; Cai, Y.; Pan, Z. Experimental study of the effective stress coefficient for coal anisotropic permeability. *Energy Fuels* **2020**, *34*, 5856–5867. [CrossRef]
32. Zhang, X.; Wu, C.; Wang, Z. Experimental study of the effective stress coefficient for coal permeability with different water saturations. *J. Pet. Sci. Eng.* **2019**, *182*, 106282. [CrossRef]
33. Zhang, G.; Ranjith, P.; Liang, W.; Haque, A.; Perera, M.; Li, D. Stress-dependent fracture porosity and permeability of fractured coal: An in-situ X-ray tomography study. *Int. J. Coal Geol.* **2019**, *213*, 103279. [CrossRef]
34. Warpinski, N.R.; Teufel, L.W. Influence of geologic discontinuities on hydraulic fracture propagation. *J. Pet. Technol.* **1987**, *39*, 209–220. [CrossRef]
35. Duan, K.; Kwok, C.Y.; Zhang, Q.; Shang, J. On the initiation, propagation and reorientation of simultaneously-induced multiple hydraulic fractures. *Comput. Geotech.* **2020**, *117*, 103226. [CrossRef]
36. Renshaw, C.E.; Pollard, D.D. An experimentally verified criterion for propagation across unbounded frictional interfaces in brittle, linear elastic materials. *Int. J. Rock Mech. Min. Sci. Geomech. Abstr.* **1995**, *32*, 237–249. [CrossRef]
37. Zhang, X.; Jeffrey, R.G.; Thiercelin, M. Deflection and propagation of fluid-driven fractures at frictional bedding interfaces: A numerical investigation. *J. Struct. Geol.* **2007**, *29*, 396–410. [CrossRef]
38. Wei, X.; Cai, M.; Kong, C.; Zhao, D. Spatiotemporal evolution analysis of multiscale fracture dynamics in hydraulic shale stimulation via integrated acoustic emission and CT imaging. *Sci. Rep.* **2025**, *15*, 44451. [CrossRef]
39. Lin, S.; Gong, D.; Li, Z.; Chen, J.; Chen, X.; Song, W. Study on fracture interference and formation mechanisms of complex fracture networks in continental shale oil horizontal well staged fracturing. *Energies* **2025**, *18*, 2862. [CrossRef]

Disclaimer/Publisher's Note: The statements, opinions and data contained in all publications are solely those of the individual author(s) and contributor(s) and not of MDPI and/or the editor(s). MDPI and/or the editor(s) disclaim responsibility for any injury to people or property resulting from any ideas, methods, instructions or products referred to in the content.